Disorder-Driven Spin-Orbital Liquid Behavior in the $Ba_3XSb_2O_9$ Materials

Andrew Smerald and Frédéric Mila
Institut de Théorie des Phénomènes Physiques, Ecole Polytechnique Fédérale de Lausanne (EPFL), CH-1015 Lausanne, Switzerland
(Received 5 June 2015; revised manuscript received 21 July 2015; published 2 October 2015)

Recent experiments on the $Ba_3XSb_2O_9$ family have revealed materials that potentially realize spin- and spin-orbital liquid physics. However, the lattice structure of these materials is complicated due to the presence of charged X^{2+}-Sb^{5+} dumbbells, with two possible orientations. To model the lattice structure, we consider a frustrated model of charged dumbbells on the triangular lattice, with long-range Coulomb interactions. We study this model using Monte Carlo simulation, and find a freezing temperature, T_{frz}, at which the simulated structure factor matches well to low-temperature x-ray diffraction data for $Ba_3CuSb_2O_9$. At $T = T_{\mathrm{frz}}$ we find a complicated "branching" structure of superexchange-linked X^{2+} clusters, which form a fractal pattern with fractal dimension $d_f = 1.90$. We show that this gives a natural explanation for the presence of orphan spins. Finally we provide a plausible mechanism by which such dumbbell disorder can promote a spin-orbital resonant state with delocalized orphan spins.

DOI: 10.1103/PhysRevLett.115.147202 PACS numbers: 75.10.Kt, 75.25.Dk, 75.47.Lx

Recently, there has been an intense search for materials exhibiting spin-liquid behavior—materials beyond the "standard model" of condensed matter physics [1]. A particularly intriguing idea is of a spin-orbital liquid, in which not only the spin but also the orbital degrees of freedom remain fluctuating down to low temperature [1–5].

The $Ba_3XSb_2O_9$ family, with $X = \mathrm{Cu}$ [6–16], Ni [17–21], Co [22–24], Mn [25,26], …, has been shown to be a promising class of materials to realize spin-liquid behavior. $Ba_3CuSb_2O_9$ has been particularly well studied, and it has been suggested that the spin and orbital degrees of freedom associated with the Cu^{2+} ions form a spin-orbital liquid state [6–16]. In the case of $Ba_3NiSb_2O_9$, the pressure-synthesized 6*H*-B structure has been proposed as an example of a spin-1 spin-liquid state [17–21].

An important starting point when trying to understand spin-liquid behavior is knowledge of the lattice structure. In $Ba_3CuSb_2O_9$ it has been suggested that the Cu^{2+} ions form a short-range honeycomb lattice [7], and theoretical approaches have therefore concentrated on Cu^{2+} plaquettes formed of several hexagons [10,12,15]. On the other hand, in the 6*H*-B phase of $Ba_3NiSb_2O_9$ it has been suggested that the Ni^{2+} ions form a triangular lattice [17].

Here we argue that in neither case is this a good starting point for theoretical investigation, and instead one should consider a disordered "branch" lattice [see Fig. 1(b)]. The evidence we present focuses in particular on $Ba_3CuSb_2O_9$, but should be applicable to other members of the $Ba_3XSb_2O_9$ family. Furthermore, we suggest that this type of correlated lattice disorder can promote spin-orbital liquid behavior.

In order to investigate the lattice structure of these materials, we solve a frustrated model of interacting X^{2+}-Sb^{5+} charged dumbbells [see Fig. 1]. We argue this is relevant to stoichiometric $X = \mathrm{Cu}$, $X = \mathrm{Ni}$ in the pressure synthesized 6*H*-B phase and potentially to pressure synthesized $X = \mathrm{Mn}$ and $X = \mathrm{Co}$.

The X^{2+}-Sb^{5+} dumbbells are surrounded by O^{2-} bioctahedra, and their constituent ions sit on the vertices of stacked triangular lattice bilayers [7], as shown in Fig. 1(a). Each dumbbell has two possible orientations with either the X^{2+} or Sb^{5+} on top. Electrostatically, the primary influence on the orientation of the dumbbells is the orientation of the other dumbbells—that is to say that the Ba^{2+}, O^{2-} and

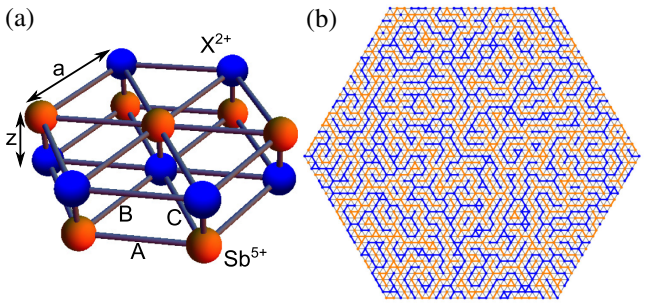

FIG. 1 (color online). Charged dumbbells on the triangular lattice. (a) X^{2+}-Sb^{5+} dumbbells of length z form a triangular lattice bilayer. There is an Ising degree of freedom associated to whether the dumbbell is orientated with X above Sb or vice versa. The equilibrium distribution of dumbbells can be mapped onto a charge model, E_{Coul} [Eq. (1)], which at low temperature orders in a stripe ground state [shown here]. (b) Material realizations of E_{Coul} [Eq. (1)] fall out of equilibrium at $T = T_{\mathrm{frz}}$, and the lattice structure can be studied by making simulations at this temperature. A snapshot of a typical lattice structure for $X = \mathrm{Cu}$ is shown, with blue and orange sites denoting different dumbbell orientations. Superexchange interactions link Cu^{2+} ions on dumbbells with the same orientation, and superexchange linked clusters are shown by blue and orange bonds.

remaining Sb^{5+} ions are electrostatically ambivalent as to the dumbbell orientation.

This leads us to consider a Coulombic charge model,

$$E_{\mathsf{Coul}} = \frac{1}{2}\sum_{i\neq j}\frac{q_i q_j}{r_{ij}}, \tag{1}$$

where $q_i = \pm 1$ is a normalized charge, i and j run over the sites of a bilayer triangular lattice [shown in Fig. 1], $r_{ij} = |\mathbf{r}_i - \mathbf{r}_j|$, and the charge distribution is constrained to have one positive and one negative charge on each dumbbell. We ignore interaction between dumbbells in different bilayers, and we provide a justification for this approximation below.

In order to relate the charge distribution following from E_{Coul} [Eq. (1)] to the lattice structure of the materials, it is necessary to understand the synthesis process. This is typically performed at high temperature ($> 1000\,^{\circ}\mathrm{C}$), and the crystals are then slowly cooled to room temperature and below [7,8]. A characteristic time scale t_{cool} can be ascribed to this cooling process, and this should be compared to t_{flip}, the characteristic time for dumbbells to reverse their orientation. Close to the synthesis temperature, we assume that $t_{\mathsf{flip}} \ll t_{\mathsf{cool}}$, and therefore the dumbbell orientation remains in thermal equilibrium as T is reduced. As the crystal is cooled, t_{flip} increases, and there is a temperature, T_{frz}, below which $t_{\mathsf{flip}} \gg t_{\mathsf{cool}}$. In this regime the dumbbell dynamics is too slow to equilibrate the system and the charge distribution is thus frozen in place. The dumbbell structure for any $T < T_{\mathsf{frz}}$ can therefore be understood from studying the equilibrium dumbbell structure at $T = T_{\mathsf{frz}}$.

The dumbbells in these materials are widely spaced, and one piece of evidence that they are dynamic at high temperature comes from the isostructural compound $Ba_3IrTi_2O_9$ [27]. Here the Ir-Ti dumbbells exhibit a markedly different low-temperature structure depending on whether the material is slowly cooled from the synthesis temperature ($1000\,^{\circ}\mathrm{C}$) or quenched.

This suggests a twofold strategy for understanding the lattice structure of these materials. (1) Simulate E_{Coul} [Eq. (1)] as a function of temperature, and, by comparison with experimental data, determine the freezing temperature, T_{frz}. (2) Simulate the model at T_{frz} in order to extract detailed information about the lattice structure for all $T < T_{\mathsf{frz}}$.

In order to simulate E_{Coul} [Eq. (1)], it is first mapped onto an Ising model on the triangular lattice using Ewald summation [28]. This leads to,

$$E_{\mathsf{Coul}} = E_0 + \frac{1}{2}\sum_{i,j}\psi_{ij}(z)\sigma_i\sigma_j, \tag{2}$$

where $\sigma_i = \pm 1$ is an Ising spin, i runs over the sites of a triangular lattice, and $\psi_{ij}(z)$ defines the interactions between sites as a function of the dumbbell size, z (see Fig. 1) [29]. For $z \to 0$, E_{Coul} [Eq. (2)] reduces to interacting Ising dipoles on the triangular lattice [31]. Here we consider $z = 0.46a$ as this is relevant to $Ba_3CuSb_2O_9$ [7].

We have performed Monte Carlo simulations of E_{Coul} [Eq. (2)] over a wide range of temperatures [29]. The ground state is sixfold degenerate, and consists of alternating stripes of $\sigma = 1$ and $\sigma = -1$, parallel to either the A, B, or C bonds [see Fig 1(a)] [32]. At $T_{\mathsf{c}}/\psi_{nn} \approx 0.19$, with the nearest-neighbor interaction $\psi_{\mathsf{nn}} \approx 0.18$ in the units of Eq. (1), there is an apparently first order phase transition into a domain wall network state, as proposed in Ref. [33] for the Ising model with further neighbor exchange interactions. We postpone a detailed description of the low-temperature behavior to another publication, and instead concentrate on the temperature region above the phase transition.

For $T > T_{\mathsf{c}}$ we perform simulations to measure the dumbbell structure factor. In the absence of interaction between bilayers, this is given by

$$S(\mathbf{q}_\perp, q_z) = \sin^2\frac{q_z}{2}\left|\sum\nolimits_i \sigma_i \exp[i\mathbf{q}_\perp\cdot\mathbf{r}_{\perp,i}]\right|^2, \tag{3}$$

where $\mathbf{r}_{\perp,i}$ measures the position of dumbbell i in the plane of the triangular lattice. Here $q_z = 2\pi z l/c$, where for $Ba_3CuSb_2O_9$ the dumbbell height is $z = 2.69$ Å, the unit cell has a height $c = 14.37$ Å and l is measured relative to the structural Bragg peaks [7]. For $l = 0$ it is not possible to observe scattering from the dumbbell structure, as there is a destructive interference between X and Sb ions within the same dumbbell. Scattering is strongest when $q_z = (2n+1)\pi$, where n is an integer, and for $n = 0$ this corresponds to $l = c/(2z) \approx 3$. Figure 2 shows $S(q_x, 2\pi/\sqrt{3}, \pi)$ at a range of temperatures, and there are diffuse peaks centered on $\mathbf{q}_\perp = (\pm 2\pi/3, 2\pi/\sqrt{3})$ [see also Fig. 3(a)].

The diffuse nature of the peaks in $S(\mathbf{q})$ [Eq. (3)] corresponds to the absence of long-range order in the dumbbell structure. The width of the peaks at half maximum gives a measure of the correlation length, ξ_{ls}. For example, for $T = 0.9\psi_{\mathsf{nn}}$ [blue curve in Fig. 2], we find $\xi_{\mathsf{ls}} \sim 2a$. In domains of this length scale the system is correlated in a stripelike pattern [see Fig. 1].

The motivation for studying the dumbbell structure factor is that it can be compared with low temperature x-ray diffraction data. This allows the freezing temperature, T_{frz}, of the sample to be determined, and then simulation at this temperature can be used to shed light on the low-temperature structure of the dumbbells in the material. One way to determine T_{frz} is to consider the ratio $R = S(0, 2\pi/\sqrt{3}, q_z)/S(2\pi/3, 2\pi/\sqrt{3}, q_z)$, since this is sensitive to temperature, as can be seen in Fig. 2. The inset to Fig. 2 shows how R increases as a function of T,

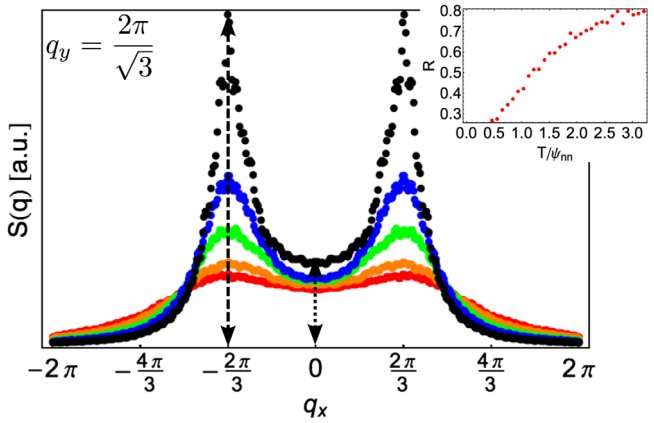

FIG. 2 (color online). The dumbbell structure factor, $S(\mathbf{q})$, as predicted by simulations of E_{Coul} [Eq. (1)]. The structure factor is plotted at a range of temperatures as a function of q_x with $q_y = 2\pi/\sqrt{3}$ and $q_z = \pi$. From top to bottom: $T/\psi_{nn} = 0.45$ (black), $T/\psi_{nn} = 0.9$ (blue), $T/\psi_{nn} = 1.4$ (green), $T/\psi_{nn} = 2.4$ (orange) and $T/\psi_{nn} = 3.2$ (red). In the inset, the ratio $R = S(0, 2\pi/\sqrt{3}, q_z)/S(2\pi/3, 2\pi/\sqrt{3}, q_z)$ (small dotted arrow compared to large dashed arrow) is plotted as a function of T.

eventually saturating in the uncorrelated, high-temperature region.

X-ray diffraction data for $Ba_3CuSb_2O_9$, which is taken from Ref. [7], are shown in Fig. 3. The value $R \approx 0.4$ is extracted, giving $T_{\text{frz}}/\psi_{nn} \approx 0.9$, and the simulated structure factor at this temperature is superposed on the experimental data, showing a good fit. The freezing temperature can be converted into Kelvin by reintroducing the dimensionful prefactors in E_{Coul} [Eq. (1)]. The only unknown is the relative permittivity ϵ_r. The dumbbells are definitely frozen at $T = 300$ K, the synthesis temperature is

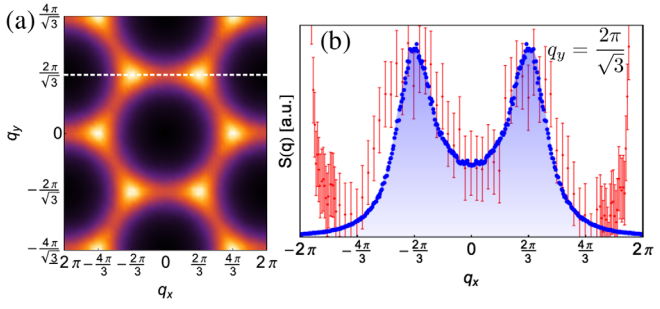

FIG. 3 (color online). Comparison between the simulated structure factor following from E_{Coul} [Eq. (1)] and x-ray diffraction experiments for $Ba_3CuSb_2O_9$ [7]. The simulation temperature, T_{frz}, is chosen so as to give the best fit to the experimental data and $L = 48$. (a) Simulated structure factor at $T = T_{\text{frz}}$ with $q_z = \pi$. (b) Cut through the simulated structure factor at $q_y = 2\pi/\sqrt{3}$ and $q_z = \pi$ [blue dots, shown by white dashed line in (a)] compared to x-ray diffraction experiments (red dots). Bragg peaks at $q_x = \pm 2\pi$ are ignored in the simulation, since these are independent of the dumbbell ordering.

> 1000 K [7], and, for T_{frz} to be within these limits, a not unreasonable value of $\epsilon_r \sim 10$ is necessary. Furthermore, the relatively high value of T_{frz} provides a justification for ignoring coupling between bilayers. However, the fact that diffuse scattering is observed at $l = 10$ suggests that some interbilayer correlation is present [7]. This is left for future investigation.

Once T_{frz} has been determined, the dumbbell structure at this effective lattice temperature can be studied in detail. The density of defect triangles, n_{tri}, on which all three dumbbells are orientated in the same direction, is shown in Fig. 4. This density is measured relative to a ferromagnetic state, in which all dumbbells are orientated in the same direction. The density, n_{tri}, increases steadily with temperature and, for $T_{\text{frz}}/\psi_{nn} = 0.9$, is given by $n_{\text{tri}} \approx 0.03$.

Also shown in Fig. 4 is the density of hexagonal plaquettes, n_{hex}, measured relative to a long-range honeycomb arrangement of dumbbells ($N/3$ plaquettes). Hexagonal plaquettes are defined as six equivalently orientated dumbbells surrounding a dumbbell of the opposite orientation. The hexagon plaquette density remains low at all temperatures, rapidly saturating at only $n_{\text{hex}} \approx 0.035$, and, for $T_{\text{frz}}/\psi_{nn} = 0.9$, is given by $n_{\text{hex}} \approx 0.025$. In Ref. [7], the presence of diffuse peaks in the x-ray diffraction spectrum at $\mathbf{q}_\perp = (2\pi/3, 2\pi/\sqrt{3})$ [see Fig. 3] was taken as proof of a short-range honeycomb arrangement of the dumbbells, since this is the wave vector at which Bragg peaks are found for a long-range ordered honeycomb arrangement. Here we have shown that such a signal arises even in the absence of a significant number of

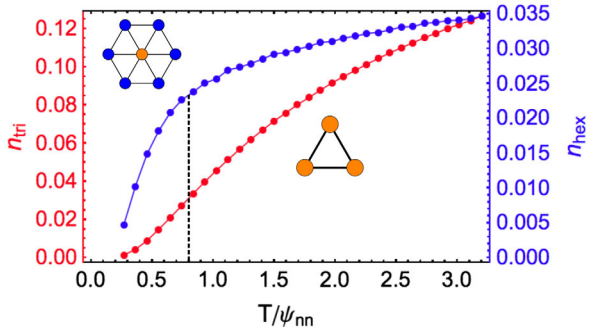

FIG. 4 (color online). Fraction of hexagonal plaquettes, n_{hex}, and defect triangles, n_{tri}, as predicted from simulations of E_{Coul} [Eq. (1)]. Hexagonal plaquettes have six dumbbells of equivalent orientation surrounding a dumbbell of the opposite orientation. The fraction of hexagonal plaquettes relative to a long range honeycomb lattice ($N/3$ plaquettes) rapidly saturates with increasing temperature at $n_{\text{hex}} \approx 0.035$ (blue, upper curve). Defect triangles have three dumbbells with the same orientation, and the fraction relative to a ferromagnetic state ($2N$ defect triangles) steadily increases with temperature (red, lower curve). The black dashed line shows $T/\psi_{nn} = 0.9$, which is believed to describe the low-temperature dumbbell structure of the $Ba_3CuSb_2O_9$ crystals studied in Ref. [7] (see Fig. 3).

hexagonal plaquettes, the building blocks of the honeycomb lattice.

How should the lattice of X ions be described, if not by a honeycomb lattice? To answer this a representative snapshot of the simulations at $T_{\mathrm{frz}}/\psi_{\mathrm{nn}} = 0.9$ is shown in Fig. 1(b). The lattice can be divided into a set of equally orientated clusters—that is clusters of neighboring dumbbells of the same orientation that are completely surrounded by dumbbells of the opposite orientation [shown joined by either blue or orange bonds in Fig. 1(b)]. Superexchange between the electronic degrees of freedom associated with the X ions predominantly occurs within these equally orientated clusters, as superexchange between oppositely orientated neighboring dumbbells is expected to be weak [7]. These superexchange-linked clusters can be seen to have a branching structure, and a wide distribution of sizes, n.

In Fig. 5 we show $p(n)$, the probability that an arbitrary site is part of an n-site cluster. For $L = 48$ ($N = 6912$) and for $10 < n < 2000$ a good fit to the numerical data is obtained using a power-law probability function, $p(n) = Cn^{1-\tau}$, with $C = 0.063$ and $\tau = 2.06$. Finite size effects result in a peak of $p(n)$ at large n and the power law also breaks down at $n \lesssim 10$, where stripelike correlations between Ising spins suppress the number of small clusters. Finite size scaling analysis of the average size of the largest cluster shows $\langle n_{\mathrm{max}} \rangle \propto L^{d_f}$, where $d_f = 1.90$ is the fractal dimension [29].

These findings match very well to percolation theory for a model of random site filling on the triangular lattice [34]. In this model the percolation threshold is at 1/2-filling, and at this critical point the exponents $\tau = 187/91 = 2.055$ and $d_f = 91/48 = 1.896$ are predicted. The close agreement

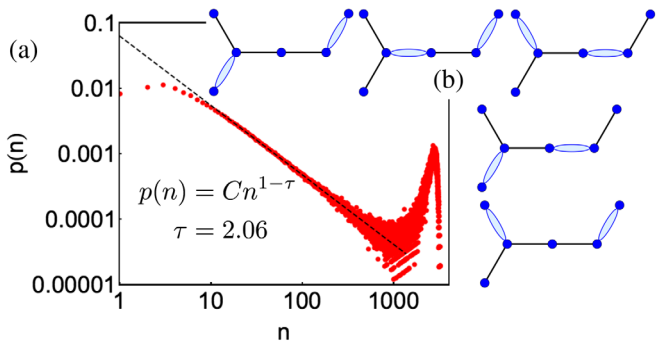

FIG. 5 (color online). Statistics of superexchange linked Cu^{2+} clusters at $T_{\mathrm{frz}}/\psi_{\mathrm{nn}} = 0.9$, measured by simulation of E_{Coul} [Eq. (1)]. (a) The probability, $p(n)$, that a site belongs to a cluster of size n ($L = 48$). For $10 < n < 1000$ a power-law distribution $p(n) = 0.063/n^{1.06}$ provides a good fit to the data. At large cluster sizes ($n > 1000$) the finite size of the simulation becomes important. (b) A six-site superexchange linked cluster of Cu^{2+} ions, with five distinct maximal dimer coverings. For geometric reasons, only four sites can be covered, leaving two monomers (orphan sites).

between these exponents and those found in the simulations suggest that the distribution of sizes of the superexchange linked clusters is at, or very close to, the percolation critical point. Thus superexchange linked clusters can be expected at all length scales [29].

It is common in the $Ba_3XSb_2O_9$ family that a sizable fraction of the electronic spins are "orphaned" and interact only weakly with the rest of the system. This is observed from a variety of experimental probes and, for $X = Cu$, the percentage of orphan spins has been measured in the range of 5%–16% [6–8,14]. Neutron scattering studies provide evidence that the Cu spins form nearest-neighbor singlet bonds at low temperature [7], leading us to consider covering the lattice in singlet dimers. Maximally covering the lattice of Cu^{2+} ions with nearest-neighbor singlet dimers leaves a number of orphan spins, due to the geometry of the clusters, and an example of this is shown in Fig. 5(b). At $T_{\mathrm{frz}}/\psi_{\mathrm{nn}} = 0.9$ the percentage of orphan spins calculated in this way is 6%, and, for $T > T_c$ this is almost independent of both the simulation temperature and the system size [29].

In this dimer picture, clusters with $n = 1$ are guaranteed to be an orphan spin, and make up about 15% of the total orphan spin population. At low temperature, ESR measures the local environment of the orphan spins [7], and is therefore biased towards a hexagonal local environment.

It is interesting to speculate about the low temperature spin-orbital state in $Ba_3CuSb_2O_9$. Theory suggests that a nearest-neighbor singlet bond is associated with a ferro-orbital alignment between the two sites [10,12,15]. In order for an orbital resonance to occur, it is therefore necessary for the system to resonate between different singlet coverings of the lattice. The mechanism for this resonance can arise directly from the superexchange interaction, or from coupling to the lattice [10,12,15].

For a typical Cu^{2+} superexchange-linked cluster found from solving E_{Coul} [Eq. (1)] at $T = T_{\mathrm{frz}}$, there are many possible maximal dimer coverings, which, for geometrical reasons, leave a number of uncovered monomer sites (orphan spins). An oscillation between different dimer coverings can equivalently be viewed as a hopping of orphan spins around the cluster. Thus resonance between different dimer configurations of a cluster not only provides a mechanism by which orbitals can resonate, but also suggests that most orphan spins will be delocalized. Since the largest superexchange linked cluster diverges in the thermodynamic limit, a resonating state of this type can be designated a spin-orbital liquid on the branch lattice. In this picture it is the correlated dumbbell disorder that promotes liquidlike behavior.

To test this picture we performed exact diagonalization for a spin-orbital Hamiltonian [12,29] on the six-site cluster shown in Fig. 5. A trial ground state wave function was constructed from the five different dimer coverings of the

cluster (shown in Fig. 5), and the overlap with the exact wave function was 0.98 [29].

In conclusion, we have considered the lattice structure of the $Ba_3XSb_2O_9$ family, which includes a number of proposed spin-liquid materials. By studying a model of charged dumbbells on the triangular lattice using Monte Carlo simulations, we find a nontrivial lattice structure [see Fig. 1(b)], in which superexchange linked clusters of X ions form a fractal branching structure. Focusing in particular on $X = \mathrm{Cu}$, which has been proposed as a spin-orbital liquid, we show that the obtained lattice structure is consistent with x-ray diffraction data. A simple model of nearest-neighbor singlet covering of the lattice results in a reasonable estimate for the number of orphan spins, and gives rise to a scenario in which correlated dumbbell disorder promotes a spin-orbital liquid state with nonlocalized orphan spins.

We thank Sergey Korshunov for very useful discussions at the beginning of this work. We also thank Luis Seabra, Ludovic Jaubert, and Nic Shannon for advice on Monte Carlo simulation. We are grateful to Satoru Nakatsuji, Hiroshi Sawa, and Naoyuki Katayama for discussions and for sharing their x-ray diffraction data. We thank the Swiss National Science Foundation and its SINERGIA network "Mott physics beyond the Heisenberg model" for financial support.

[1] C. Lacroix, P. Mendels, and F. Mila, *Introduction to Frustrated Magnetism* (Springer, New York, 2011).
[2] S. Ishihara, M. Yamanaka, and N. Nagaosa, Phys. Rev. B **56**, 686 (1997).
[3] G. Khaliullin and S. Maekawa, Phys. Rev. Lett. **85**, 3950 (2000).
[4] D. I. Khomskii and M. V. Mostovoy, J. Phys. A **36**, 9197 (2003).
[5] P. Corboz, M. Lajkó, A. M. Läuchli, K. Penc, and F. Mila, Phys. Rev. X **2**, 041013 (2012).
[6] H. D. Zhou, E. S. Choi, G. Li, L. Balicas, C. R. Wiebe, Y. Qiu, J. R. D. Copley, and J. S. Gardner, Phys. Rev. Lett. **106**, 147204 (2011).
[7] S. Nakatsuji, K. Kuga, K. Kimura, R. Satake, N. Katayama, E. Nishibori, H. Sawa, R. Ishii, M. Hagiwara, F. Bridges, T. U. Ito, W. Higemoto, Y. Karaki, M. Halim, A. A. Nugroho, J. A. Rodriguez-Rivera, M. A. Green, and C. Broholm, Science **336**, 559 (2012).
[8] J. A. Quilliam, F. Bert, E. Kermarrec, C. Payen, C. Guillot-Deudon, P. Bonville, C. Baines, H. Luetkens, and P. Mendels, Phys. Rev. Lett. **109**, 117203 (2012).
[9] Y. Ishiguro, K. Kimura, S. Nakatsuji, S. Tsutsui, A. Q. R. Baron, T. Kimura, and Y. Wakabayashi, Nat. Commun. **4**, 2022 (2013).
[10] J. Nasu and S. Ishihara, Phys. Rev. B **88**, 094408 (2013).
[11] N. Katayama, K. Kimura, Y. Han, J. Nasu, N. Drichko, Y. Nakanishi, M. Halim, Y. Ishiguro, R. Satake, E. Nishibori, M. Yoshizawa, T. Nakano, Y. Nozue, Y. Wakabayashi, S. Ishihara, M. Hagiwara, H. Sawa, and S. Nakatsuji, Proc. Natl. Acad. Sci. U.S.A. **112**, 9305 (2015).
[12] A. Smerald and F. Mila, Phys. Rev. B **90**, 094422 (2014).
[13] K. V. Shanavas, Z. S. Popović, and S. Satpathy, Phys. Rev. B **89**, 085130 (2014).
[14] S.-H. Do, J. van Tol, H. D. Zhou, and K.-Y. Choi, Phys. Rev. B **90**, 104426 (2014).
[15] J. Nasu and S. Ishihara, Phys. Rev. B **91**, 045117 (2015).
[16] Y. Han, M. Hagiwara, T. Nakano, Y. Nozue, K. Kimura, M. Halim, and S. Nakatsuji, arXiv:1508.01653.
[17] J. G. Cheng, G. Li, L. Balicas, J. S. Zhou, J. B. Goodenough, C. Xu, and H. D. Zhou, Phys. Rev. Lett. **107**, 197204 (2011).
[18] C. Xu, F. Wang, Y. Qi, L. Balents, and M. P. A. Fisher, Phys. Rev. Lett. **108**, 087204 (2012).
[19] S. Bieri, M. Serbyn, T. Senthil, and P. A. Lee, Phys. Rev. B **86**, 224409 (2012).
[20] G. Chen, M. Hermele, and L. Radzihovsky, Phys. Rev. Lett. **109**, 016402 (2012).
[21] K. Hwang, T. Dodds, S. Bhattacharjee, and Y. B. Kim, Phys. Rev. B **87**, 235103 (2013).
[22] Y. Shirata, H. Tanaka, A. Matsuo, and K. Kindo, Phys. Rev. Lett. **108**, 057205 (2012).
[23] T. Susuki, N. Kurita, T. Tanaka, H. Nojiri, A. Matsuo, K. Kindo, and H. Tanaka, Phys. Rev. Lett. **110**, 267201 (2013).
[24] G. Koutroulakis, T. Zhou, Y. Kamiya, J. D. Thompson, H. D. Zhou, C. D. Batista, and S. E. Brown, Phys. Rev. B **91**, 024410 (2015).
[25] Z. Tian, C. Zhu, Z. Ouyang, J. Wang, W. Tong, Y. Liu, Z. Xia, and S. Yuan, J. Magn. Magn. Mater. **360**, 10 (2014).
[26] Z. Tian, Q. Guo, Z. Ouyang, G. Du, W. Tong, J. Wang, and S. Yuan, Solid State Commun. **191**, 66 (2014).
[27] T. Dey, A. V. Mahajan, P. Khuntia, M. Baenitz, B. Koteswararao, and F. C. Chou, Phys. Rev. B **86**, 140405 (2012).
[28] A. Grzybowski, E. Gwóźd ź, and A. Bródka, Phys. Rev. B **61**, 6706 (2000).
[29] See Supplemental Material at http://link.aps.org/supplemental/10.1103/PhysRevLett.115.147202 for further information concerning the interaction matrix $\psi_{ij}(z)$, the statistics of superexchange linked clusters, the orphan spins and the diagonalization of a spin-orbital Hamiltonian, which includes Ref. [30].
[30] W. Zhang, T. M. Garoni, and Y. Deng, Nucl. Phys. **B814**, 461 (2009).
[31] U. K. Rößler, J. Appl. Phys. **89**, 7033 (2001).
[32] In a 3D model of charged dumbbells we expect the ground state to retain a stripe pattern within the layers. For nearest-neighbor interlayer coupling, the stripe state gives the best possible interlayer energy consistent with the absence of defect triangles in the plane. Other simple 2D states, such as the honeycomb, give much worse interlayer energies. Thus we expect that the 3D model shows the same qualitative features as the 2D model.
[33] S. E. Korshunov, Phys. Rev. B **72**, 144417 (2005).
[34] D. Stauffer and A. Aharony, *Introduction to Percolation Theory* (Taylor and Francis, London, 1992).